JACS
JOURNAL OF THE AMERICAN CHEMICAL SOCIETY
Communication
pubs.acs.org/JACS

Photoinduced Solid State Conversion of a Radical σ-Dimer to a π-Radical Pair

Hoa Phan,[†] Kristina Lekin,[‡] Stephen M. Winter,[‡] Richard T. Oakley,*[,‡] and Michael Shatruk*[,†]

[†]Department of Chemistry and Biochemistry, Florida State University, Tallahassee, Florida 32306, United States
[‡]Department of Chemistry, University of Waterloo, Waterloo, Ontario N2L 3G1, Canada

Supporting Information

ABSTRACT: Irradiation in the solid state of the hypervalent 4c-6e S···S–S···S bridged σ-dimer of a bisdithiazolyl radical leads to its photodissociation into a pair of π-radicals. The transformation has been monitored by optical spectroscopy, single crystal X-ray diffraction, and magnetic susceptibility measurements. As a result of the large electronic reorganization involved in the dimer-to-radical interconversion, the photogenerated $S = 1/2$ radical state is remarkably thermally stable, persisting to 242 K before reverting to the $S = 0$ dimer.

Photoinduced switching of the magnetic state of molecular materials holds the potential for applications in data storage, high-speed sensing, and radiation detectors.[1] Within this context one of the most well-known and heavily studied photomagnetic phenomena is light-induced excited spin state trapping (LIESST) found for some transition metal complexes.[2−4] Essentially, the LIESST effect involves a change in the population of the t_{2g} and e_g orbitals, a so-called spin crossover (SCO) between high and low spin states.[5] In the solid state this configurational change leads to variations in bond lengths which can be as large as 0.2 Å,[6] but no formal bond breaking or making occurs during the spin transition. As a result, the activation barrier for relaxation of the high spin state is typically small, and the photoinduced high-spin product rarely remains stable above 100 K,[7] the highest T_{LIESST} being (to our knowledge) 180 K.[7b]

In principle, photoinduced spin state changes in all-organic molecular materials can also serve as a basis for magnetic switching,[8] but utilization of these effects in solid state devices remains a challenge. For example, while photochemically driven singlet–triplet interconversions have been extensively studied, the resulting triplet states are generally short-lived.[9] In solution, greater stability has been achieved when the spin state changes are accompanied by large conformational changes,[10] but this strategy is not easily transferable to the confines of the crystal environment. By contrast, the thermally induced solid state interconversion of a diamagnetic radical dimer ($S = 0$) to a pair of stable paramagnetic radicals (each $S = 1/2$) is well documented, and such systems have been shown to exhibit thermal hysteresis and even wide regimes of bistability.[11,12] In one case photoinduced dimer-radical interconversion within the thermally bistable region has also been reported.[13] However, the photoinduced low-temperature conversion of a radical dimer to a pair of radicals and subsequent trapping of the resulting open shell state is hitherto unobserved.

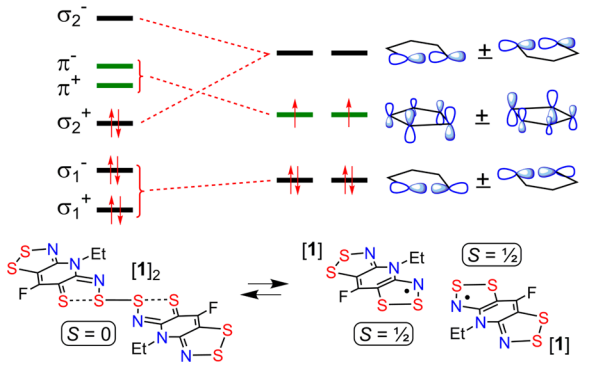

Figure 1. Configurational $(\sigma_2^+)^2 \leftrightarrow (\pi^+)(\pi^-)$ change accompanying the interconversion of the 4c-6e hypervalent S···S–S···S σ-dimer $[\mathbf{1}]_2$ and a pair of π-radicals $[\mathbf{1}]$.

Recently we reported the preparation of the heterocyclic bisdithiazolyl radical $[\mathbf{1}]$ (Figure 1), which crystallizes in two modifications,[14] one consisting (at room temperature) of diamagnetic dimers $[\mathbf{1}]_2$ in which radical pairs are linked by hypervalent 4-center 6-electron (4c-6e) S···S–S···S σ-bonds.[15] This arrangement is unusual, in that dissociation of the dimer to a pair of radicals is symmetry forbidden, involving a configurational $(\sigma_2^+)^2 \leftrightarrow (\pi^+)(\pi^-)$ change.[14] Nonetheless, the thermodynamic balance between open and closed shell forms is relatively small; DFT estimates place the bond dissociation enthalpy ΔH_{diss} near 11 kcal mol^{-1}.[16] Consistently, variable temperature magnetic and crystallographic measurements revealed that the dimer could be thermally converted, within the same space group, to the radical at 380 K, a dimer-to-radical interconversion that displayed thermal hysteresis with a small (5 K) window of magnetic bistability. The same structural transformation could also be driven by pressurization to ∼0.8 GPa at ambient temperature. Here we report that the solid state interconversion $[\mathbf{1}]_2 \rightarrow 2\,[\mathbf{1}]$ can also be effected photochemically. Moreover, the photogenerated radical displays an unprecedented thermal stability, not reverting to the closed shell dimer until 242 K.

Initial experiments to explore the possibility of the photoinduced conversion of $[\mathbf{1}]_2 \rightarrow 2\,[\mathbf{1}]$ involved examination of the evolution of the solid state transmission optical

Received: June 4, 2013
Published: October 9, 2013

   dx.doi.org/10.1021/ja4055806 | J. Am. Chem. Soc. 2013, 135, 15674−15677

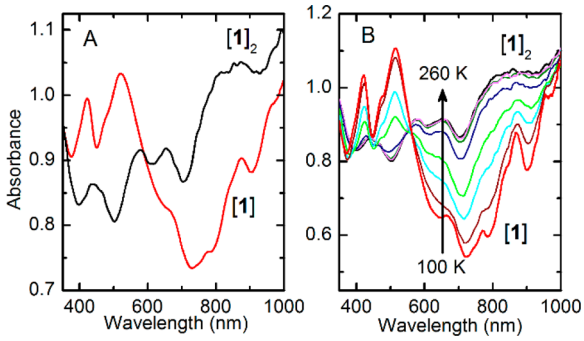

Figure 2. (A) Optical absorption spectra recorded on a thin film of $[\mathbf{1}]_2$ at 100 K before and after irradiation with white light (black and red curves, respectively). (B) Evolution of the absorption spectrum obtained after irradiation of the thin film of $[\mathbf{1}]_2$ at 100 K with a 650-nm laser, and subsequent warming to 260 K. The spectra shown after the one at 100 K (red line) were recorded from 230 to 260 K with 5-K steps at a heating rate of 0.2 K min^{-1}.

absorption spectrum of $[\mathbf{1}]_2$ under irradiation. Figure 2A shows the optical spectrum of a microcrystalline film of $[\mathbf{1}]_2$ at 100 K, both before (black curve) and after (red curve) the sample was irradiated with white light (~10 mW cm^{-2}) for 4 min. The broad absorption of $[\mathbf{1}]_2$ in the 600−800 nm range was substantially diminished after irradiation, while new bands appeared at 422 and 515 nm signifying the generation of the radical [**1**]. Based on these observations, and to minimize the absorption of light by the photogenerated [**1**], we subsequently used a 650-nm laser for variable-temperature optical, crystallographic, and photomagnetic experiments. Thus, in a second optical absorption experiment, a microcrystalline film of $[\mathbf{1}]_2$ was irradiated with the 650-nm laser (~25 mW cm^{-2}) for 20 s at 100 K, and the resulting optical absorption spectrum was monitored as a function of increasing temperature. The spectrum of the radical [**1**] generated by laser irradiation (red curve in Figure 2B) remained essentially unchanged until 230 K, above which temperature the broad absorption in the 600−800 nm range gradually reappeared and the bands at 422 and 515 nm vanished (Figure 2B). Spectra recorded at 250 K and above matched the original spectrum of $[\mathbf{1}]_2$.

Given the use of low-power continuous irradiation and the high temperature (>380 K) required to induce the thermal conversion, the possibility of photothermal effects[17] is unlikely. That the mechanism is predominantly photochemical is further supported by the quasi-linear dependence of the conversion on power density at 100 K at low power (Figure S1).

Relaxation of the photoinduced state was examined by monitoring the isothermal decay of the 510 nm band at different temperatures. The photogenerated radical [**1**] remained stable for prolonged periods at temperatures below 220 K. Even at 220 K, the relaxation is very slow, amounting only to ~13% after 4 h. Thereafter the relaxation rate constant increases with increasing temperature, as expected for a thermally activated process. A fit of the relaxation kinetics between 230 and 250 K (Figure 3A) to a single-exponential decay was only partially satisfactory, as the relaxation tends to proceed somewhat faster toward the end of the decay, a result attributable to cooperative solid-state effects. Arrhenius analysis of the temperature dependence of the derived relaxation rate k_{RD} (Figure 3B) afforded a relaxation barrier E_{act} = 19.6(7) kcal mol^{-1}.

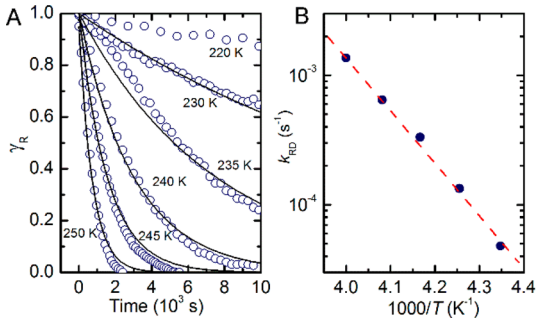

Figure 3. (A) Mole fraction γ_R of photogenerated [**1**] as a function of time at different temperatures, along with fitted (single exponential) curves. (B) Log plot of relaxation rate constants k_{RD} as a function of inverse temperature (with linear fit in red).

Visualization of the structural changes associated with the photoinduced dissociation was achieved by single-crystal X-ray diffraction.[18] To this end a needle-like crystal of $[\mathbf{1}]_2$ was cooled to 100 K and irradiated with a 650-nm laser for 4 h. Analysis of diffraction data collected subsequently at 100 K confirmed a quantitative transformation $[\mathbf{1}]_2 \rightarrow 2\,[\mathbf{1}]$ within the common space group $P2_1/c$; difference electron-density maps did not reveal any significant peaks that would suggest the presence of a residual fraction of dimer. As may be seen in Figure 4, which compares the crystal and molecular structures

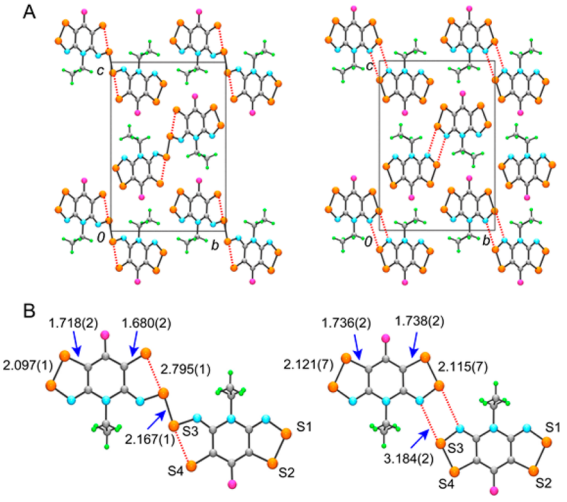

Figure 4. (A) Unit cell diagrams of $[\mathbf{1}]_2$ and of photogenerated [**1**], viewed along the *a* axis. (B) Selected distances (in Å) within the dimer and radical pair. Both structures were determined at 100 K.

of the dimer and the photogenerated radical pair, both determined at 100 K, the loss of the interdimer S3−S3′ bond (2.167(1) Å) is accompanied by slippage about the crystallographic inversion center, to form a pair of radicals weakly linked by a pair of long S3···N3′ intermolecular contacts (3.184(2) Å). At the same time the long transannular S3···S4 hypervalent contact (2.795(1) Å) closes to a value (2.115(7) Å) near that observed for S1−S2 (2.121(7) Å), and the thione C2−S4 double bond (1.680(2) Å) expands to 1.738(2) Å, a value akin to that seen for the S2−C4 single bond (1.736(2) Å). Overall, the unit cell and molecular metrics for the photoinduced radical [**1**] are in keeping with those found from high pressure (0.98 GPa) and high temperature (380 K) measurements.[14]

dx.doi.org/10.1021/ja4055806 | J. Am. Chem. Soc. 2013, 135, 15674−15677

For photomagnetic measurements a microcrystalline film of $[\mathbf{1}]_2$ was placed on a flexible diamagnetic tape mounted on the end of a quartz rod connected to an optical fiber. The sample so prepared was lowered into a SQUID magnetometer at 300 K, cooled to 10 K, and irradiated with a 650-nm laser, which resulted in an increase of the observed magnetic response, in agreement with the photogeneration of paramagnetic $[\mathbf{1}]$ from diamagnetic $[\mathbf{1}]_2$. The irradiation was stopped after 2 h, and the magnetic susceptibility (χ) was measured in a warming mode under an applied field H = 0.1 T. The plot in Figure 5 shows

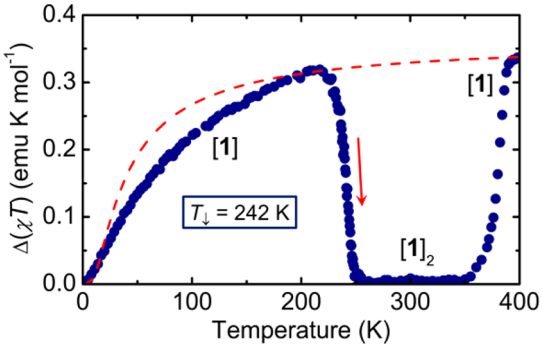

Figure 5. Change in χT (at H = 0.1 T) upon warming a thin film of $[\mathbf{1}]_2$ after irradiation with λ = 650 nm at 10 K (blue curve). The sample was warmed at a rate of 3 K min^{-1} at 5–220 K, 0.2 K min^{-1} at 220–260 K, 3 K min^{-1} at 260–360 K, and 1 K min^{-1} at 360–400 K. The dashed red line tracks the value of χT for $[\mathbf{1}]$ estimated from exact diagonalization simulations based on exchange energies obtained from DFT calculations.

the difference in the χT product of the irradiated sample, and the original sample cooled down in the dark. Presented in such a way, the data allow accurate subtraction of the diamagnetic contribution from the sample holder and the intrinsic diamagnetism of the sample. (The absolute values of the measured moments before and after irradiation are shown in Figure S2.) The χT value gradually increases on warming, suggesting the presence of antiferromagnetic (AFM) exchange coupling between radicals. Field-dependent magnetization (M) measurements taken at 1.8 K support this conclusion, as a very slow increase in M is observed with increasing field (Figure S3). Indeed the value of M of ca. 0.07 μ_B at 7 T is still much smaller than the saturation value of 1 μ_B expected for an S = 1/2 radical, which is consistent with significant antiferromagnetic coupling between the radicals.

In accord with the optical measurements, χT decreases, first gradually above 230 K, and then abruptly, with an inflection temperature $T_{\downarrow}$ = 242 K. This behavior is consistent with thermally activated relaxation of the metastable radical to the thermodynamically favored dimer $[\mathbf{1}]_2$. Above 260 K, the observed χT value matches that measured for the sample of $[\mathbf{1}]_2$ prior to irradiation. Further heating results in an abrupt increase in χT around 380 K, which is consistent with the thermally induced process reported earlier.[14] The $\Delta(\chi T)$ value attained at 400 K is nearly the same as the maximum $\Delta(\chi T)$ observed for the photogenerated $[\mathbf{1}]$ at 225 K, which indicates that the conversion $[\mathbf{1}]_2 \rightarrow 2\ [\mathbf{1}]$ is essentially quantitative.

To analyze the magnetic response of $[\mathbf{1}]$ in the low temperature (<230 K) region, we carried out a series of broken symmetry density functional theory (DFT) calculations[19] at the UB3LYP/6-311G(d,p) level[20] to estimate the magnitude of the pairwise magnetic exchange coupling

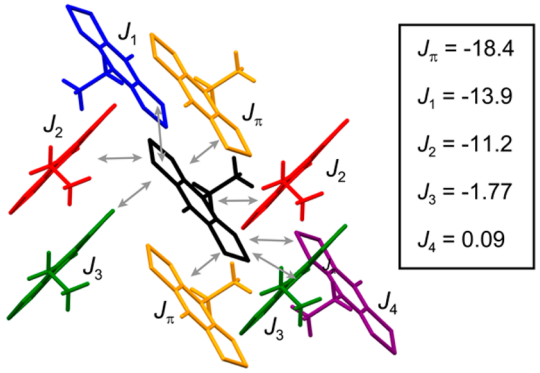

Figure 6. Definition of contacts for pairwise magnetic exchange interactions J_{1-4} and J_π in the crystal structure of photogenerated $[\mathbf{1}]$ at 100 K, and UB3LYP/6-311G(d,p) calculated values (in cm^{-1}).

constants (J) within the photoinduced crystal structure. With reference to the Heisenberg Hamiltonian $H_{ex} = -2J\ \{S_1 \cdot S_2\}$, exchange energies J_{1-4} and J_π for interacting pairs of radicals (Figure 6) were computed using single-point energies of the lowest triplet E_{TS} and broken symmetry singlet E_{BSS} states and their respective $\langle S^2 \rangle$ expectation values. As expected, the dominant exchange interactions are antiferromagnetic, corresponding to coupling along the π-stacks ($J_\pi = -18.4$ cm^{-1}) and between the formerly dimerized radical pairs ($J_1 = -13.9$ cm^{-1}). The entire set of calculated J-values was then used to generate a 16-site exact diagonalization simulation[21] of the bulk magnetic susceptibility of $[\mathbf{1}]$ as a function of temperature. The resulting theoretically predicted $\chi T(T)$ function, shown in Figure 5 as a dashed red line, is in good qualitative agreement with the experimentally observed data over the same range. Extrapolation of the function to higher temperatures suggests that the residual effects of AFM exchange interactions may slightly suppress the χT value even of the thermally generated radical (above 380 K).

The stability of the photogenerated radical $[\mathbf{1}]$, which persists to $T_{\downarrow}$ = 242 K, provides an interesting contrast to the behavior of most transition-metal based SCO materials, for which the photoinduced high spin state rarely survives above 100 K.[7b,22] This remarkable behavior may be related to the unusual 4c-6e hypervalent linkage in $[\mathbf{1}]_2$.[14] Most radical dimers, be they linked by localized or delocalized interactions,[23] are well described in terms of a direct coupling of singly occupied orbitals on two radicals; that is, the radical and dimer forms have the same state symmetry. By contrast, interconversion of the hypervalent σ-bonded dimer $[\mathbf{1}]_2$ and two π-radicals $[\mathbf{1}]$ requires a configurational $(\sigma_2^+)^2 \leftrightarrow (\pi^+)(\pi^-)$ change (Figure 1).[14] A configurational reorganization is also found in SCO materials, so that both here and in SCO systems the transformation is symmetry forbidden, guaranteeing an inherent activation barrier at the molecular level. However, where the processes differ is in the magnitude of the structural changes involved, that is, >0.6 Å for the back-reaction $2\ [\mathbf{1}] \rightarrow [\mathbf{1}]_2$ compared to ≤0.2 Å for metal–ligand distances of an SCO metal ion.[7] Under these circumstances a higher thermal stability for the trapped photoinduced radical state $[\mathbf{1}]$ is to be expected. We believe our findings augur well for the use of trapped photoinduced radicals in the design of new radical-based materials displaying a magneto-optical response. Moreover, given that heterocyclic radicals of this type can be conductive[24] and also form magnetically ordered[25] structures, opportunities may emerge for the development of radical/dimer systems

dx.doi.org/10.1021/ja4055806 | J. Am. Chem. Soc. 2013, 135, 15674–15677

capable of responding to optical stimuli in both magnetic and electrical channels.[11d,26]

■ ASSOCIATED CONTENT

Supporting Information

Full citations for refs 20 and 21. Details of optical, magnetic, crystallographic measurements, and theoretical modeling of magnetic data. Details of crystallographic data collection and structure refinement of $[\mathbf{1}]_2$ and photogenerated $[\mathbf{1}]$, both at 100 K, in CIF format. This material is available free of charge via the Internet at http://pubs.acs.org.

■ AUTHOR INFORMATION

Corresponding Authors

oakley@uwaterloo.ca
shatruk@chem.fsu.edu.

Notes

The authors declare no competing financial interest.

■ ACKNOWLEDGMENTS

We thank the National Science Foundation (Grant CHE-0911109 to M.S.) and the Natural Sciences and Engineering Research Council of Canada (NSERCC) for partial financial support. We also acknowledge the NSERCC for a Graduate Scholarship to S.M.W. and a Vanier Scholarship to K.L., as well as the Vietnam Ministry of Education and Training for a VIED Scholarship to H.P.

■ REFERENCES

(1) (a) Feringa, B., Ed. *Molecular Switches*, 2nd ed.; Wiley-VCH: Weinheim, 2001. (b) Nasu, K., Ed. *Photoinduced Phase Transitions*; World Scientific Publishing: Singapore, 2004. (c) Létard, J.-F.; Guionneau, P.; Goux-Capes, L. *Top. Curr. Chem.* **2004**, *235*, 221. (d) Bousseksou, A.; Molnár, G.; Salmon, L.; Nicolazzi, W. *Chem. Soc. Rev.* **2011**, *40*, 3313.

(2) (a) Decurtins, S.; Gütlich, P.; Köhler, C. P.; Spiering, H.; Hauser, A. *Chem. Phys. Lett.* **1984**, *105*, 1. (b) Decurtins, S.; Gütlich, P.; Hasselbach, K. M.; Hauser, A.; Spiering, H. *Inorg. Chem.* **1985**, *24*, 2174.

(3) Sato, O.; Iyoda, T.; Fujishima, A.; Hashimoto, K. *Science* **1996**, *272*, 704.

(4) (a) Hauser, A. *Top. Curr. Chem.* **2004**, *234*, 155. (b) Sato, O.; Tao, J.; Zhang, Y.-Z. *Angew. Chem., Int. Ed.* **2007**, *46*, 2152.

(5) (a) Gütlich, P.; Goodwin, H. A., Eds. *Spin Crossover in Transition Metal Compounds I–III*: Springer: Berlin, Heidleberg, 2004. (b) Halcrow, M. A., Ed. *Spin Crossover Materials: Properties and Applications*; J. Wiley & Sons: Chichester, U.K., 2013.

(6) Guionneau, P.; Marchivie, M.; Bravic, G.; Létard, J. F.; Chasseau, D. *Top. Curr. Chem.* **2004**, *234*, 97.

(7) (a) Varret, F.; Boukheddaden, K.; Chastanet, G.; Paradis, N.; Létard, J.-F. *Eur. J. Inorg. Chem.* **2013**, 763. (b) Li, D.; Clérac, R.; Roubeau, O.; Harté, E.; Mathonière, C.; Le Bris, R.; Holmes, S. M. *J. Am. Chem. Soc.* **2008**, *130*, 252.

(8) (a) Ratera, I.; Veciana, J. *Chem. Soc. Rev.* **2012**, *41*, 303. (b) Nakatsuji, S. *Chem. Soc. Rev.* **2004**, *33*, 348.

(9) (a) Zhu, Z.; Bally, T.; Stracener, L. L.; McMahon, R. *J. Am. Chem. Soc.* **1999**, *121*, 2863. (b) Sajimon, M. C.; Ramaiah, D.; Suresh, C. H.; Adam, W.; Lewis, F. D.; George, M. V. *J. Am. Chem. Soc.* **2007**, *129*, 9439. (c) Günaydın-Sen, Ö.; Fosso-Tande, J.; Chen, P.; White, J. L.; Allen, T. L.; Cherian, J.; Tokumoto, T.; Lahti, P. M.; McGill, S.; Harrison, R. J.; Musfeldt, J. S. *J. Chem. Phys.* **2011**, *135*, 241101. (d) Modarelli, D. A.; Lahti, P. M. *J. Am. Chem. Soc.* **1991**, *113*, 6329.

(10) (a) Teki, Y.; Miyamoto, S.; Nakatsuji, M.; Miura, Y. *J. Am. Chem. Soc.* **2001**, *123*, 294. (b) Ratera, I.; Ruiz-Molina, D.; Vidal-Gancedo, J.; Novoa, J. J.; Wurst, K.; Letard, J.-F.; Rovira, C.; Veciana, J. *Chem.—Eur. J.* **2004**, *10*, 603. (c) Matsuda, K.; Irie, M. *J. Am. Chem. Soc.* **2000**, *122*, 7195. (d) Matsuda, K.; Irie, M. *Chem.—Eur. J.* **2001**, *7*, 3466.

(11) (a) Barclay, T. M.; Cordes, A. W.; George, N. A.; Haddon, R. C.; Itkis, M. E.; Mashuta, M. S.; Oakley, R. T.; Patenaude, G. W.; Reed, R. W.; Richardson, J. F.; Zhang, H. *J. Am. Chem. Soc.* **1998**, *120*, 352. (b) Fujita, W.; Awaga, K. *Science* **1999**, *286*, 261. (c) McManus, G. D.; Rawson, J. M.; Feeder, N.; van Duijn, J.; McCinnes, E. J. L.; Novoa, J. J.; Burriel, R.; Palacio, F.; Oliete, P. *J. Mater. Chem.* **2001**, *11*, 1992. (d) Itkis, M. E.; Chi, X.; Cordes, A. W.; Haddon, R. C. *Science* **2002**, *296*, 1443. (e) Brusso, J. L.; Clements, O. P.; Haddon, R. C.; Itkis, M. E.; Leitch, A. A.; Oakley, R. T.; Reed, R. W.; Richardson, J. F. *J. Am. Chem. Soc.* **2004**, *126*, 14692. (f) Pal, S. K.; Bag, P.; Sarkar, A.; Chi, X.; Itkis, M. E.; Tham, F. S.; Donnadieu, B.; Haddon, R. C. *J. Am. Chem. Soc.* **2010**, *132*, 17258.

(12) (a) Hicks, R. G. *Nat. Chem.* **2011**, *3*, 189. (b) Hicks, R. G., Ed. *Stable Radicals: Fundamentals and Applied Aspects of Odd-Electron Compounds*: J. Wiley & Sons: Chichester, U.K., 2010. (c) Rawson, J. M.; Hayward, J. J. In *Spin-Crossover Materials: Properties and Applications*; Halcrow, M. A., Ed.; J. Wiley & Sons: Chichester, 2013; p 235.

(13) Matsuzaki, H.; Fujita, W.; Awaga, K.; Okamoto, H. *Phys. Rev. Lett.* **2003**, *91*, 017403.

(14) Lekin, K.; Winter, S. M.; Downie, L. E.; Bao, X.; Tse, J. S.; Desgreniers, S.; Secco, R. A.; Dube, P. A.; Oakley, R. T. *J. Am. Chem. Soc.* **2010**, *132*, 16212.

(15) (a) Nakanishi, W.; Hayashi, S.; Arai, T. *Chem. Commun.* **2002**, 2416. (b) Nakanishi, W.; Hayashi, S.; Morinaka, S.; Sasamori, T.; Tokitoh, N. *New J. Chem.* **2008**, *32*, 1881.

(16) Beer, L.; Brusso, J. L.; Haddon, R. C.; Itkis, M. E.; Kleinke, H.; Leitch, A. A.; Oakley, R. T.; Reed, R. W.; Richardson, J. F.; Secco, R. A.; Yu, X. *J. Am. Chem. Soc.* **2005**, *127*, 1815.

(17) Cobo, S.; Ostrovskii, D.; Bonhommeau, S.; Vendier, L.; Molnár, G.; Salmon, L.; Tanaka, K.; Bousseksou, A. *J. Am. Chem. Soc.* **2008**, *130*, 9019.

(18) Crystal data for $[\mathbf{1}]_2$ at 100 K: monoclinic $P2_1/c$, a = 5.2962(6) Å, b = 11.3270(13) Å, c = 17.3316(18) Å, β = 105.020(3)°, V = 1004.2(2) Å^3, Z = 4. Crystal data for $[\mathbf{1}]$ at 100 K: monoclinic $P2_1/c$, a = 5.1383(8) Å, b = 11.4110(17) Å, c = 17.384(3) Å, β = 105.192(4)°, V = 983.7(3) Å^3, Z = 4. The crystallographic information files are available through the Cambridge Crystallographic Data Centre, reference numbers CCDC-935135 for $[\mathbf{1}]_2$ and CCDC-930339 for $[\mathbf{1}]$.

(19) (a) Noodleman, L. *J. Chem. Phys.* **1981**, *74*, 5737. (b) Noodleman, L.; Davidson, E. R. *Chem. Phys.* **1986**, *109*, 131. (c) Nagao, H.; Nishino, M.; Shigeta, Y.; Soda, T.; Kitagawa, Y.; Onishi, T.; Yoshika, Y.; Yamaguchi, K. *Coord. Chem. Rev.* **2000**, *198*, 265. (d) Deumal, M.; Robb, M. A.; Novoa, J. J. *Prog. Theor. Chem. Phys.* **2007**, *16*, 271.

(20) Frisch, M. J.; et al. *Gaussian 09*, revision A.02; Gaussian Inc.: 2009.

(21) Exact diagonalization simulations employed the ALPS library. See: Bauer, B.; et al. *J. Stat. Mech.* **2011**, P05001.

(22) Shimamoto, N.; Ohkoshi, S.; Sato, O.; Hashimoto, K. *Inorg. Chem.* **2002**, *41*, 678.

(23) (a) Beneberu, H. Z.; Tian, Y.-H.; Kertesz, M. *Phys. Chem. Chem. Phys.* **2012**, *14*, 10713. (b) Haynes, D. A. *CrystEngComm* **2011**, *13*, 4793.

(24) (a) Yu, X.; Mailman, A.; Lekin, K.; Assoud, A.; Robertson, C. M.; Noll, B. C.; Campana, C. F.; Howard, J. A. K.; Dube, P. A.; Oakley, R. T. *J. Am. Chem. Soc.* **2012**, *134*, 2264. (b) Mailman, A.; Winter, S. M.; Yu, X.; Robertson, C. M.; Yong, W.; Tse, J. S.; Secco, R. A.; Liu, Z.; Dube, P. A.; Howard, J. A. K.; Oakley, R. T. *J. Am. Chem. Soc.* **2012**, *134*, 9886.

(25) (a) Robertson, C. M.; Leitch, A. A.; Cvrkalj, K.; Reed, R. W.; Myles, D. J. T.; Dube, P. A.; Oakley, R. T. *J. Am. Chem. Soc.* **2008**, *130*, 8414. (b) Leitch, A. A.; Brusso, J. L.; Cvrkalj, K.; Reed, R. W.; Robertson, C. M.; Dube, P. A.; Oakley, R. T. *Chem. Commun.* **2007**, 3368.

(26) Miller, J. S. *Angew. Chem., Int. Ed.* **2003**, *42*, 27.